JACS
JOURNAL OF THE AMERICAN CHEMICAL SOCIETY
Article
pubs.acs.org/JACS

High-Mobility Field-Effect Transistors from Large-Area Solution-Grown Aligned C_{60} Single Crystals

Hanying Li,[†,⊥] Benjamin C-K. Tee,[‡] Judy J. Cha,[§] Yi Cui,[§] Jong Won Chung,[∥] Sang Yoon Lee,[∥] and Zhenan Bao*[,†]

[†]Department of Chemical Engineering, [‡]Department of Electrical Engineering, and [§]Department of Materials Science and Engineering, Stanford University, Stanford, California 94305, United States

[∥]Display Device Laboratory, Materials and Device Institute, Samsung Advanced Institute of Technology, Samsung Electronics Company, Ltd., Youngin 446-712, Korea

Supporting Information

ABSTRACT: Field-effect transistors based on single crystals of organic semiconductors have the highest reported charge carrier mobility among organic materials, demonstrating great potential of organic semiconductors for electronic applications. However, single-crystal devices are difficult to fabricate. One of the biggest challenges is to prepare dense arrays of single crystals over large-area substrates with controlled alignment. Here, we describe a solution processing method to grow large arrays of aligned C_{60} single crystals. Our well-aligned C_{60} single-crystal needles and ribbons show electron mobility as high as 11 $cm^2V^{-1}s^{-1}$ (average mobility: 5.2 ± 2.1 $cm^2V^{-1}s^{-1}$ from needles; 3.0 ± 0.87 $cm^2V^{-1}s^{-1}$ from ribbons). This observed mobility is ~8-fold higher than the maximum reported mobility for solution-grown n-channel organic materials (1.5 $cm^2V^{-1}s^{-1}$) and is ~2-fold higher than the highest mobility of any n-channel organic material (~6 $cm^2V^{-1}s^{-1}$). Furthermore, our deposition method is scalable to a 100 mm wafer substrate, with around 50% of the wafer surface covered by aligned crystals. Hence, our method facilitates the fabrication of large amounts of high-quality semiconductor crystals for fundamental studies, and with substantial improvement on the surface coverage of crystals, this method might be suitable for large-area applications based on single crystals of organic semiconductors.

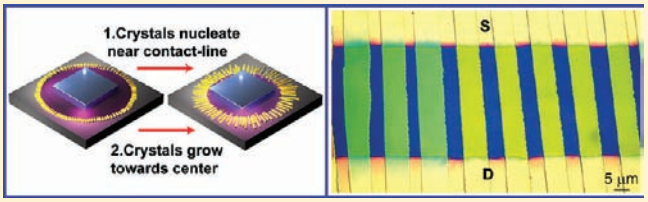

INTRODUCTION

Organic field-effect transistors (FETs) are promising for flexible, low-cost, and lightweight electronic applications, such as complementary circuits,[1−4] displays,[5,6] and sensors.[7−11] Organic thin films have been widely used to fabricate FET devices due to their facile processability in large areas. The charge mobility of p-channel organic thin-film FETs has reached up to 23.2 $cm^2V^{-1}s^{-1}$.[12−16] For n-channel organic thin-film FETs, vapor-deposited devices exhibit mobility as high as 6 $cm^2V^{-1}s^{-1}$,[17,18] while solution-processed ones have lower mobility of ~1 $cm^2V^{-1}s^{-1}$.[2,19−21] Organic single crystals, in theory, are ideal charge-transport media, with fewer structural defects and thus better electronic performance than the thin-film counterparts.[22] Experimentally, single crystals of organic semiconductors exhibit hole mobility up to 40 $cm^2V^{-1}s^{-1}$ and electron mobility as high as 6 $cm^2V^{-1}s^{-1}$.[22−33] Although the charge carrier mobility of single-crystal devices is much higher than that of thin-film FETs, single-crystal devices are mostly limited to fundamental charge-transport research because individual devices are usually fabricated manually, and it is difficult to scale-up for technological applications. In contrast to continuous thin-films where devices can be defined anywhere, crystal growth location is stochastic in nature, and yet, position registration between crystals and electrodes is crucial to make electronic contacts. Therefore, various attempts have been made to achieve high-throughput controlled placement of single crystals. Crystals can be either selectively grown where the electrodes are located[26,34,35] or aligned and subsequently transferred onto the pattern electrodes.[23] In this work, we report a facile approach to deposit well-aligned C_{60} single crystals on substrates as large as a 100 mm wafer. FETs based on these crystals exhibit unprecedented electron mobility above 10 $cm^2V^{-1}s^{-1}$.

EXPERIMENTAL SECTION

Crystals were grown in situ on substrates for FETs. Divinyltetramethyldisiloxane bis(benzocyclobutene) (BCB, Dow Chemicals) thin layers were spin coated from a mesitylene (Fluka) solution (V_{BCB}:$V_{mesitylene}$ = 1: 30) and thermally cross-linked on a hot plate in a N_2 glovebox. A C_{60} (Alfa Aesar) solution (20 μL) was dropped onto a BCB-covered highly doped silicon substrate (1 cm^2) with 300 nm SiO_2. A piece of silicon wafer (0.4 × 0.4 cm^2, pinner) was placed on the substrate to pin the solution droplet (Figure 1). The silicon substrate with the droplet was placed on a Teflon slide inside a Petri dish (35 × 10 mm) sealed with parafilm. Crystals formed on the silicon substrate after the solvent slowly evaporated on a hot plate of 30 ± 1 °C. Needle-shaped crystals were grown from *m*-xylene (Sigma-Aldrich) with a C_{60} concentration ([C_{60}]) of 0.4 mg mL^{-1}, and the

Received: November 6, 2011
Published: January 6, 2012

   dx.doi.org/10.1021/ja210430b | J. Am. Chem.Soc. 2012, 134, 2760−2765

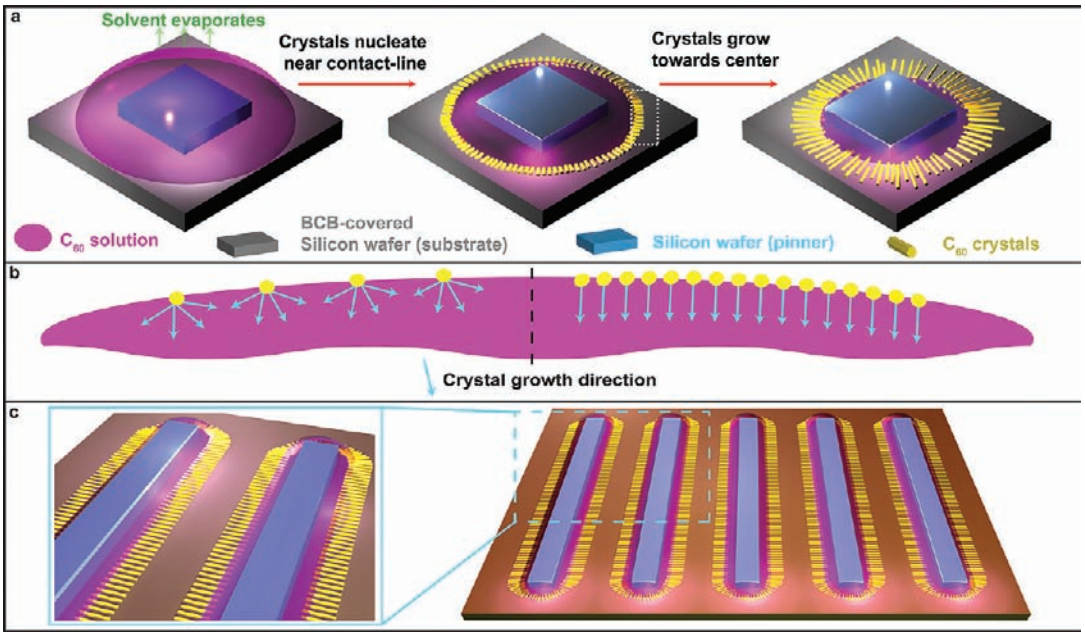

Figure 1. Schematic representations of the DPC method. (a) An organic semiconductor droplet pinned by a silicon wafer. As the solvent evaporates slowly, the crystals of the organic semiconductors nucleate near the contact line of the droplet. Subsequently, the nuclei grow along the receding direction (toward the center) of the droplet. (b) A magnified view of a white-marked area in (a), highlighting the contact line where a high nucleation density (right side) leads to unidirectional crystallization along the receding direction of the droplet, while a low nucleation density (left side) results in nondirectional crystallization. (c) DPC can be scaled up by using multiple pinners with larger sizes. Elongation of the pinner leads to unidirectional parallel alignment of the crystals.

solution dried out in ~2 h. Ribbon-shaped crystals were from mixed solvents of *m*-xylene and carbon tetrachloride (CCl_4, Sigma-Aldrich) (V_{CCl4}:$V_{m\text{-}xylene}$ = 4:3; [C_{60}] = 0.4 mg mL^{-1}), and the solution dried out in ~1 h. The volume ratio (4:3) was chosen as more *m*-xylene favored the growth of needle crystals and more carbon tetrachloride favored disk-shaped crystals. The crystals grown at varied volume ratio will be published later. For crystallization in a 100 mm wafer scale, 1.5 mL of solutions was dropped on a BCB-covered silicon wafer with pinners (0.4 cm wide) placed at 1 cm intervals. The morphology and crystalline structures were characterized by optical microscopy (OM, Leica, DM4000m), atomic force microscopy (AFM, Digital Instruments MMAFM-2), and transmission electron microscopy (TEM, FEI Tecnai F20, 200 keV for the needles; FEI Titan 80-300, 80 keV for the ribbons; 80 keV was necessary for the ribbons to minimize the beam damage). FETs were constructed in a bottom-gated configuration by depositing top-contact source and drain electrodes (80 nm Au), with channel length of 50 μm and width of 1 mm. Current−voltage characteristics of the devices were measured in a N_2 glovebox using a Keithley 4200-SCS semiconductor parameter analyzer. The measured capacitance of the BCB-covered SiO_2/Si substrates was 10 nF/cm^2, and this value was used for mobility calculation. For statistics, data of crystal heights and electron mobility are presented as mean ± SD.

RESULTS

Many approaches have been used to align organic semiconductors.[36] Among them, zone casting,[37] dip coating,[38] and solution sheared deposition[39] showed promising results for preparing aligned crystals with large grains over large areas directed by (concentration and/or temperature) gradients at the receding meniscus. Adopting a similar principle of alignment, we designed a simple droplet-pinned crystallization (DPC) method (Figure 1a) with several advantages over the previous methods. The operating principle of this approach is as follows: During drying of a droplet of a semiconductor solution on a substrate, crystals nucleate near the contact line and grow along the receding direction (toward the center) of the droplet. Using this method, well-aligned C_{60} needle and ribbon crystals were prepared (Figure 2a,d). We have also successfully applied this method to other organic semiconductor materials, such as 6,13-bis(triisopropyl-silylethynyl) pentacene (TIPS-pentacene)[40] (Figure S1, Supporting Information).

Two important requirements need to be satisfied to induce alignment. First, a high nuclei density (i.e., high solution concentration) is required to introduce a mass depletion between the nuclei. Only the nuclei with a preferential growth direction along the droplet receding direction (i.e., mass transport direction) can continuously evolve into larger crystals (Figure 1b and Figure S2, Supporting Information). However, at low nucleation density, crystals grow in random directions. Second, a steady contact line receding is needed. A drying droplet on a substrate typically will slide to a corner or edge, usually due to a slight tilt of the substrate. This sliding disrupts the steady receding of the droplet, resulting in uncontrolled alignment (Figure S3, Supporting Information). In order to avoid sliding, we placed a small piece of Si wafer (which we termed a pinner) at the center of the droplet, leading to a steady receding contact line (Figure 1a). We notice that Takeya group also used a piece of solid to sustain a inclined solution film and achieved oriented organic crystals.[41]

During the DPC process, the shape, size, and location of the droplet are determined by those of the pinner, which gives the DPC method several remarkable advantages. First, DPC is easily scalable. The pinners can be patterned over a large area with a controlled density. We scaled the processed area up to a 100 mm wafer area (Figures 1c and 3). Around 50% of the wafer surface was covered by aligned crystals. This area fraction will further increase if we decrease the size of the pinners. We envision that an even larger processed area should be achievable. Second, DPC can be used to define the location

dx.doi.org/10.1021/ja210430b | J. Am. Chem.Soc. 2012, 134, 2760−2765

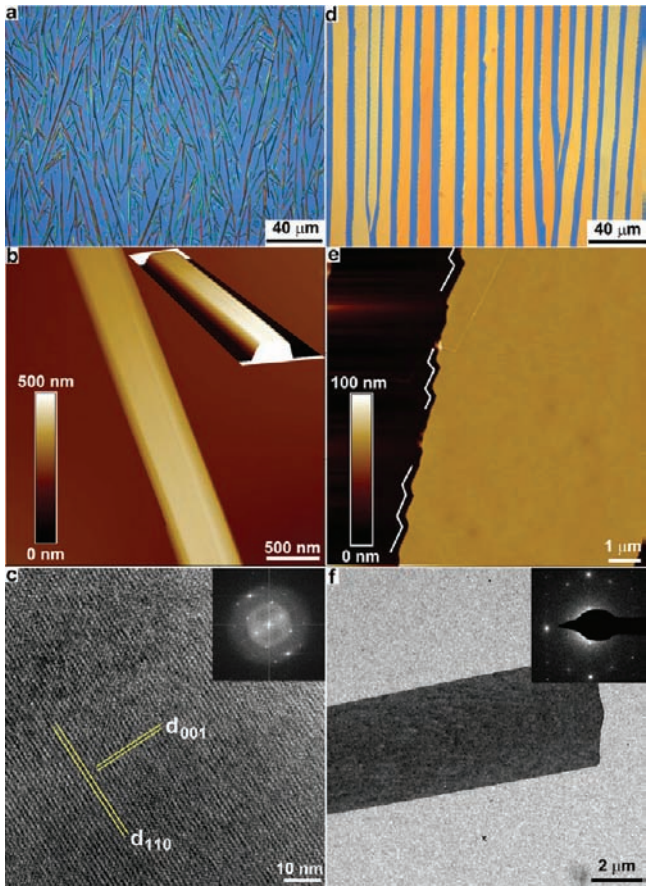

Figure 2. Morphologies and crystalline structures of well-aligned C_{60} needle (a–c) and ribbon (d–f) crystals prepared by the DPC method. (a,d) OM images of well-aligned C_{60} needle and ribbon crystals. (b) AFM image of a needle crystal showing faceted shape; (inset) 3-D view of image (b). Height of 20 needle crystals was measured, giving an average of 175 ± 80 nm (SD). (c) High-resolution TEM image of a needle crystal, showing a regular 2-D lattice of C_{60}·*m*-xylene single crystals; (inset) fast Fourier transform (FFT) of (c). (e) AFM image of a ribbon crystal. White lines highlight the faceted edges. Height of 10 ribbon crystals was measured, giving an average of 57 ± 7 nm (SD). (f) TEM image of a ribbon; (inset) SAED pattern containing a single set of spots, indicating the single crystallinity of the ribbon. SAED at different locations of the ribbon showed identical patterns.

of the aligned crystals, which is important toward making complex circuits. Since the locations of the droplets are dictated by our pinners, we could therefore achieve crystallization of desired patterns (Figures 1c and 3). Based on our DPC method, we have been able to position both p- and n-channel organic semiconductors on a common substrate to fabricate complementary circuits.

After obtaining the crystals, we proceed to characterize the morphologies and crystalline structures of the crystals. C_{60} needle crystals were grown from a solution of *m*-xylene on BCB-covered SiO_2/Si substrates (Figure 2a). Previously, crystals grown from the same solvent on SiO_2/Si substrates exhibited a similar needle shape, albeit without alignment.[42,43] Here, by using DPC, we obtained well-aligned crystals with lengths up to 200 μm (Figure 2a). Instead of a bare SiO_2/Si substrate, we used thermally cross-linked BCB to eliminate the electron traps arising from the surface hydroxyl group on SiO_2.[17,44,45] AFM shows a faceted shape and very smooth surfaces (rms roughness ∼1 nm) from the needles (Figure 2b), indicative of crystalline structures. This was further confirmed by TEM. TEM shows a regular two-dimensional (2-D) lattice image viewed down the $[1\bar{1}0]$ zone axis of C_{60} single crystals (Figure 2c). The crystalline structure is consistent with the previously reported hexagonal structure of C_{60}·*m*-xylene crystals grown from the same solvent.[42] The presence of the *m*-xylene solvent molecules inside the crystals is also evidenced from the Raman peak shifts (Figure S4, Supporting Information).

Besides the needle-shaped crystals, well-aligned ribbon crystals were also prepared from a mixture of solvents (*m*-xylene and CCl_4). The flat 2-D ribbon-shaped crystals promise a higher current output from the resulting FETs as they have a larger contact area (with the electrodes and the dielectric of the devices), compared to the needle crystals discussed earlier. We used mixed solvents to optimize the shape and coverage of the crystals.[43] With a volume ratio of 4:3 (CCl_4:*m*-xylene), long ribbons of several hundred micrometers in length were obtained with thickness of 57 ± 7 nm (Figure 2d,e and Figure 3). AFM images show faceted edges (Figure 2e, white lines) and smooth surfaces with a rms roughness (∼0.15 nm) much smaller than the diameter of C_{60} molecules (∼0.7 nm).[46] These faceted morphologies imply single crystallinity that is further confirmed by selected area electron diffraction (SAED) showing a single set of spots (Figure 2f). SAED patterns from multiple areas of the same ribbon are identical, supporting the single-crystalline nature.

The alignment facilitates FET fabrication as electrodes can be easily deposited perpendicular to the aligned crystals. FETs were constructed based on the well-aligned needles and ribbons in a bottom-gated configuration, by depositing Au top-contact source and drain electrodes, with channel length (L) of 50 μm and width (W) of 1 mm (Figure 4a, b inset, and d). For each type of crystals, 60 devices from 4 substrates were tested under N_2 atmosphere, and the saturation regime electron mobility was calculated. The typical transfer characteristics of the devices are shown in Figure 4b,e, exhibiting excellent gate modulation. Since the crystals do not fully cover the channels, the active channel width was measured from the contacting area of the crystals that cross the source and drain electrodes (Figure 4a,d). The mobility was gate bias dependent (Figure S6a,d, Supporting Information), and we extracted the mobility by linear fitting of $(I_{DS})^{1/2}$ vs V_G curves in a range of about 10 Vs. For the needles, an average electron mobility (μ) of 5.2 ± 2.1 $cm^2V^{-1}s^{-1}$ (Figure 4c), on-to-off current ratios (I_{on}/I_{off}) > 10^5, and threshold voltages (V_T) between 15 to 43 V were achieved. For the ribbons, average μ of 3.0 ± 0.87 $cm^2V^{-1}s^{-1}$ (Figure 4f), I_{on}/I_{off} > 10^6, and V_T between 36 to 85 V were obtained. The variations of the μ and V_T values are associated with the slightly different orientation of the crystals with respect to the electrodes and can be minimized by reducing channel geometry (W and L). We also assessed the bias stress effects of the devices. Transfer characteristics were recorded before and after the devices were biased in the "on" state for one hour. The extracted μ and V_T values before and after bias stress show a small variation below 10%.

DISCUSSION

The electron mobility of the C_{60} needle and ribbon single crystals is among the highest values for organic materials. The highest electron mobility we achieved is 11 $cm^2V^{-1}s^{-1}$ from the needles (Figure S5, Supporting Information), which is ∼2-fold higher than the maximum reported electron mobility (6 $cm^2V^{-1}s^{-1}$ from FETs based on vapor-deposited thin films)

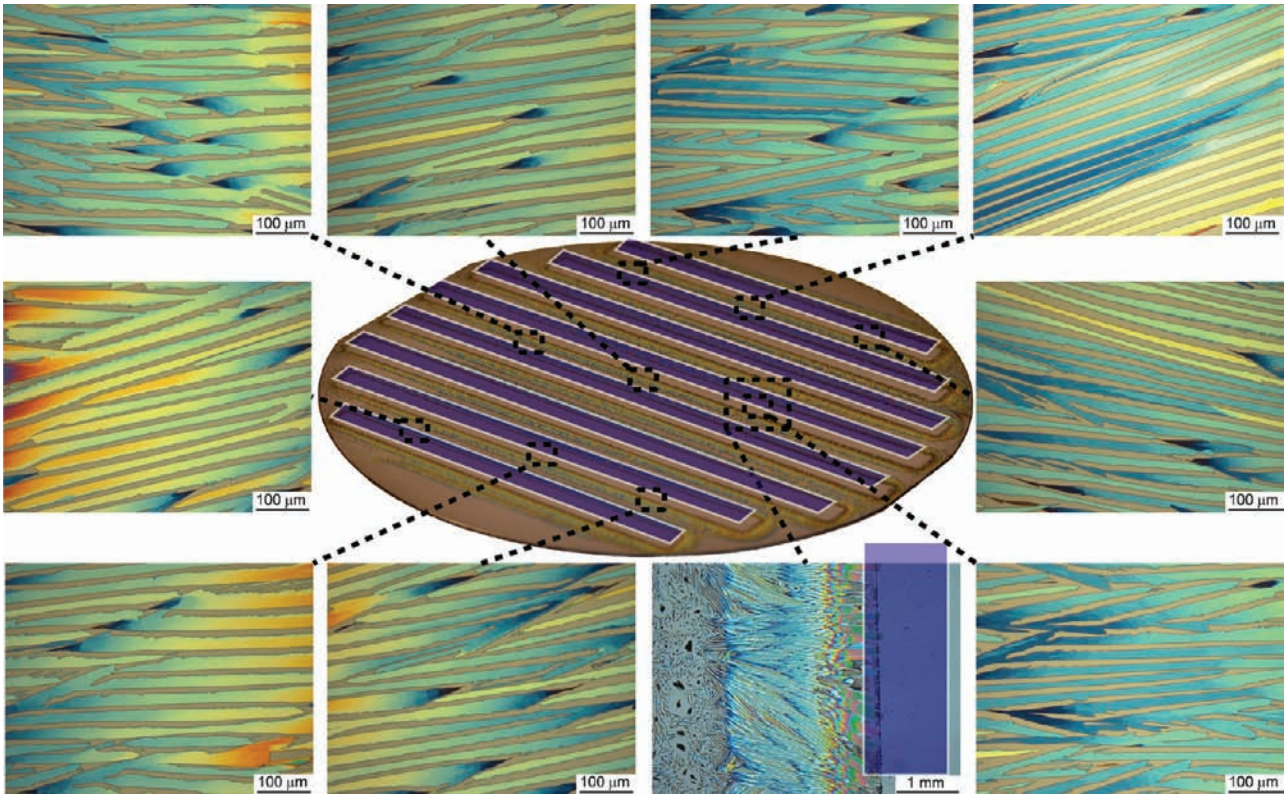

Figure 3. OM images of horizontally aligned ribbon crystals grown on a 100 mm silicon wafer. An image of the wafer is shown in the middle. The stripe pattern, highlighted in purple, is where we placed the silicon pinners to direct the crystal alignment. Across the wafer, crystals are aligned roughly perpendicular to the long axis of the pinners.

for C_{60}-based FETs.[17] To the best of our knowledge, this is the highest field-effect electron mobility for organic semiconductors demonstrating, for the first time, electron mobility above 10 $cm^2V^{-1}s^{-1}$. We attribute the high mobility to the single-crystallinity as well as the good electrical contacts at both the crystal−dielectric and the crystal−electrode interfaces. Even though C_{60} single crystals have been previously grown from solutions and vapors,[17,34,42,43] the single-crystal FETs are difficult to fabricate, and only in one case[34] were the FETs reported with a relatively low electron mobility of 0.03 $cm^2V^{-1}s^{-1}$. Our DPC method facilitates device fabrication for two reasons: First, DPC allows in situ growth of single crystals on the device substrates to form an intimate interface with the dielectric. Second, our crystals grown by DPC are thin and long enough so that we were able to use a top-contact-electrode structure to guarantee an excellent electrical contact between the crystals and electrodes. Despite high mobility in inert atmosphere, the mobility of these devices decreased in air, which has also been reported for C_{60} thin films.[47] For example, the mobility of one of the ribbon-based FET decreased about 85% after 1 day exposure in air. The ambient instability of C_{60} is due to its low electron affinity and can be improved by doping or incorporation of interfacial electric dipoles.[45,47]

Compared to the C_{60} needles, the C_{60} ribbons show a slightly lower mobility and higher threshold voltage. The difference of the device performance is mainly due to the different chemical and crystalline structures of the needles and ribbons. Although they are both single crystalline in nature, the crystals incorporate solvent molecules (*m*-xylene and/or CCl_4) during their formation,[42,43] resulting in two different structures. Raman spectrum indicates the incorporation of *m*-xylene inside the needle crystals (Figure S4, Supporting Information) and energy dispersive X-ray analysis (EDX) shows the presence of the CCl_4 molecules inside the ribbon crystals (Figure S8, Supporting Information). Further study of X-ray diffraction on large crystals is required to resolve the molecular packing in the crystals. The solvent incorporation might introduce charge traps to induce the relatively high threshold voltages, hysteresis of transfer characteristics (Figure S6b,e, Supporting Information), and reduced mobility in the linear region (about 15−30% of the saturation mobility). Despite the lower mobility, the ribbon-based devices have crystals covering the channel more densely and exhibit higher current output on the order of 0.1 mA (Figure 4d,e), which is significant for practical circuit applications where a large fan-out is typically present in multistage logic circuits.

■ CONCLUSION

In summary, we have demonstrated a highly efficient, yet simple, approach to rapidly prepare well-aligned C_{60} needle- and ribbon-shaped single crystals. This approach also offers scalability as we can easily process over large-area substrates, such as a 100 mm wafer. The long, aligned single crystals connect the source and drain electrodes of FETs to allow electron transport inside a single-crystalline domain with unprecedented electron mobility as high as 11 $cm^2V^{-1}s^{-1}$. This single-crystal deposition method could be potentially extended to other crystalline organic semiconductors to prepare thin layers of single crystals in situ on the substrates for devices. Our method will facilitate fabrication of various devices with organic semiconductor single crystals, such as circuits and solar

dx.doi.org/10.1021/ja210430b | J. Am. Chem.Soc. 2012, 134, 2760−2765

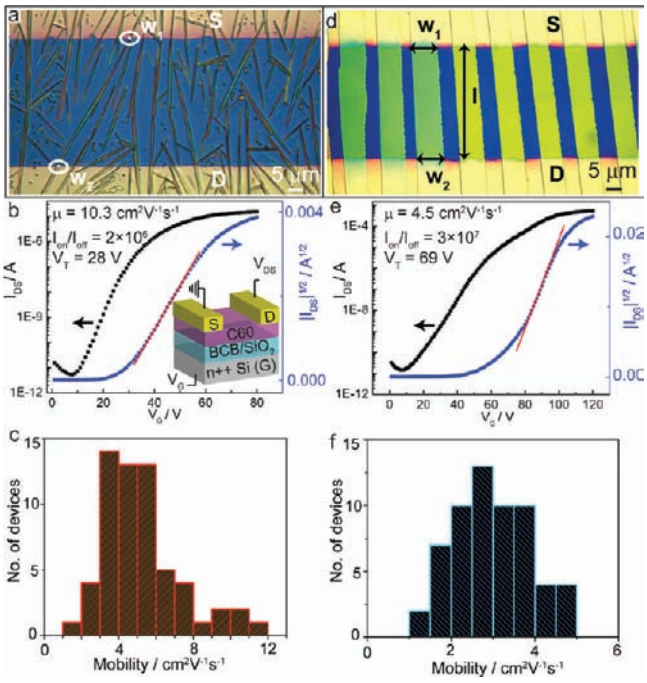

Figure 4. FET characteristics of C_{60} needle (a-c) and ribbon (d-f) crystals. (a, d) OM images showing crystals between source (S) and drain (D) electrodes. The active charge transport channel dimensions (W and L) were corrected by the equations: $W = \Sigma(w_1+w_2)/2$; $L = l$. L was measured from the real channel length and W was measured from the contacting area of the crystals that cross the S and D electrodes. For the device with the highest mobility, the channel width measurement from OM images was reconfirmed by using SEM images with a higher spatial resolution (Figure S5, Supporting Information). (b, e) Typical transfer characteristics. Inset: a schematic representation of the FET configuration, where S is the source, D the drain and G the gate. Device characteristics (μ, I_{on}/I_{off} and V_T) are also shown. The μ is calculated using the corrected W and L. For the device shown in (b), W/L = 8.7 μm/40 μm (12 needles); for (e), W/L = 817 μm/47 μm. Typical hysteresis and output characteristics are shown in Figure S6, Supporting Information. (c, f) Histogram of the electron mobility calculated using corrected W and L from 60 devices. The electron mobility calculated using uncorrected W and L is shown in Figure S7, Supporting Information.

cells,[48,49] for fundamental understanding as well as high performance.

■ ASSOCIATED CONTENT

Ⓢ Supporting Information

Complete ref 5, images of crystals, FET characteristics, Raman spectrum, and EDX spectrum. This material is available free of charge via the Internet at http://pubs.acs.org.

■ AUTHOR INFORMATION

Corresponding Author

zbao@stanford.edu

Present Address

[⊥]Department of Polymer Science and Engineering, Zhejiang University, Hangzhou 310027, P. R. China.

■ ACKNOWLEDGMENTS

This work is supported by National Science Foundation (NSF), Division of Materials Research (DMR) solid-state chemistry under award DMR-0705687-002, Air Force Office of Scientific Research (AFOSR) (grant no. FA9550-09-1-0256), and the Samsung Advanced Institute of Technology. B.C-K.T. acknowledges support from a National Science Scholarship from the Agency for Science, Technology, and Research (A*STAR), Singapore. We thank Dr. J.B-H. Tok, Dr. P. Wei, and Dr. H.B. Akkerman for discussions. We also thank W. Ito for taking photographs of the silicon wafer.

■ REFERENCES

(1) Sekitani, T.; Zschieschang, U.; Klauk, H.; Someya, T. *Nat. Mater.* **2010**, *9*, 1015.
(2) Yan, H.; Chen, Z. H.; Zheng, Y.; Newman, C.; Quinn, J. R.; Dotz, F.; Kastler, M.; Facchetti, A. *Nature* **2009**, *457*, 679.
(3) Klauk, H.; Zschieschang, U.; Pflaum, J.; Halik, M. *Nature* **2007**, *445*, 745.
(4) Crone, B.; Dodabalapur, A.; Lin, Y. Y.; Filas, R. W.; Bao, Z.; LaDuca, A.; Sarpeshkar, R.; Katz, H. E.; Li, W. *Nature* **2000**, *403*, 521.
(5) Gelinck, G. H.; et al. *Nat. Mater.* **2004**, *3*, 106.
(6) Rogers, J. A.; Bao, Z.; Baldwin, K.; Dodabalapur, A.; Crone, B.; Raju, V. R.; Kuck, V.; Katz, H.; Amundson, K.; Ewing, J.; Drzaic, P. *Proc. Natl. Acad. Sci. U.S.A.* **2001**, *98*, 4835.
(7) Mannsfeld, S. C. B.; Tee, B. C. K.; Stoltenberg, R. M.; Chen, C.; Barman, S.; Muir, B. V. O.; Sokolov, A. N.; Reese, C.; Bao, Z. N. *Nat. Mater.* **2010**, *9*, 859.
(8) Sekitani, T.; Yokota, T.; Zschieschang, U.; Klauk, H.; Bauer, S.; Takeuchi, K.; Takamiya, M.; Sakurai, T.; Someya, T. *Science* **2009**, *326*, 1516.
(9) Roberts, M. E.; Sokolov, A. N.; Bao, Z. N. *J. Mater. Chem.* **2009**, *19*, 3351.
(10) Sokolov, A. N.; Roberts, M. E.; Johnson, O. B.; Cao, Y. D.; Bao, Z. N. *Adv. Mater.* **2010**, *22*, 2349.
(11) Someya, T.; Kato, Y.; Sekitani, T.; Iba, S.; Noguchi, Y.; Murase, Y.; Kawaguchi, H.; Sakurai, T. *Proc. Natl. Acad. Sci. U.S.A.* **2005**, *102*, 12321.
(12) Tsao, H. N.; Cho, D. M.; Park, I.; Hansen, M. R.; Mavrinskiy, A.; Yoon, D. Y.; Graf, R.; Pisula, W.; Spiess, H. W.; Müllen, K. *J. Am. Chem. Soc.* **2011**, *133*, 2605.
(13) Payne, M. M.; Parkin, S. R.; Anthony, J. E.; Kuo, C. C.; Jackson, T. N. *J. Am. Chem. Soc.* **2005**, *127*, 4986.
(14) Wang, C.-H.; Hsieh, C.-Y.; Hwang, J.-C. *Adv. Mater.* **2011**, *23*, 1630.
(15) Wang, Y.; Acton, O.; Ting, G.; Weidner, T.; Shamberge, P. J.; Ma, H.; Ohuchi, F. S.; Castner, D. G.; Jen, A. K. Y. *Org. Electron.* **2010**, *11*, 1066.
(16) Virkar, A.; Mannsfeld, S.; Oh, J. H.; Toney, M. F.; Tan, Y. H.; Liu, G. Y.; Scott, J. C.; Miller, R.; Bao, Z. *Adv. Funct. Mater.* **2009**, *19*, 1962.
(17) Anthopoulos, T. D.; Singh, B.; Marjanovic, N.; Sariciftci, N. S.; Ramil, A. M.; Sitter, H.; Colle, M.; de Leeuw, D. M. *Appl. Phys. Lett.* **2006**, *89*, 213504.
(18) Shukla, D.; Nelson, S. F.; Freeman, D. C.; Rajeswaran, M.; Ahearn, W. G.; Meyer, D. M.; Carey, J. T. *Chem. Mater.* **2008**, *20*, 7486.
(19) Polander, L. E.; Tiwari, S. P.; Pandey, L.; Seifried, B. M.; Zhang, Q.; Barlow, S.; Risko, C.; Bredas, J. L.; Kippelen, B.; Marder, S. R. *Chem. Mater.* **2011**, *23*, 3408.
(20) Wu, Q. H.; Li, R. J.; Hong, W.; Li, H. X.; Gao, X. K.; Zhu, D. B. *Chem. Mater.* **2011**, *23*, 3138.
(21) Soeda, J.; Uemura, T.; Mizuno, Y.; Nakao, A.; Nakazawa, Y.; Facchetti, A.; Takeya, J. *Adv. Mater.* **2011**, *23*, 3681.
(22) Podzorov, V.; Menard, E.; Borissov, A.; Kiryukhin, V.; Rogers, J. A.; Gershenson, M. E. *Phys. Rev. Lett.* **2004**, *93*, 086602.
(23) Oh, J. H.; Lee, H. W.; Mannsfeld, S.; Stoltenberg, R. M.; Jung, E.; Jin, Y. W.; Kim, J. M.; Yoo, J. B.; Bao, Z. N. *Proc. Natl. Acad. Sci. U.S.A.* **2009**, *106*, 6065.
(24) Sundar, V. C.; Zaumseil, J.; Podzorov, V.; Menard, E.; Willett, R. L.; Someya, T.; Gershenson, M. E.; Rogers, J. A. *Science* **2004**, *303*, 1644.

(25) Molinari, A. S.; Alves, H.; Chen, Z.; Facchetti, A.; Morpurgo, A. F. *J. Am. Chem. Soc.* **2009**, *131*, 2462.
(26) Nakayama, K.; Hirose, Y.; Soeda, J.; Yoshizumi, M.; Uemura, T.; Uno, M.; Li, W.; Kang, M.; Yamagishi, M.; Okada, Y.; Miyazaki, E.; Nakazawa, Y.; A., N.; Takimiya, K.; Takeya, J. *Adv. Mater.* **2011**, *23*, 1626.
(27) Jurchescu, O. D.; Popinciuc, M.; van Wees, B. J.; Palstra, T. T. M. *Adv. Mater.* **2007**, *19*, 688.
(28) Takeya, J.; Yamagishi, M.; Tominari, Y.; Hirahara, R.; Nakazawa, Y.; Nishikawa, T.; Kawase, T.; Shimoda, T.; Ogawa, S. *Appl. Phys. Lett.* **2007**, *90*, 102120.
(29) Menard, E.; Podzorov, V.; Hur, S. H.; Gaur, A.; Gershenson, M. E.; Rogers, J. A. *Adv. Mater.* **2004**, *16*, 2097.
(30) Reese, C.; Bao, Z. N. *Mater. Today* **2007**, *10*, 20.
(31) Minemawari, H.; Yamada, T.; Matsui, H.; Tsutsumi, J.; Haas, S.; Chiba, R.; Kumai, R.; Hasegawa, T. *Nature* **2011**, *475*, 364.
(32) Islam, M. M.; Pola, S.; Tao, Y. T. *Chem. Commun.* **2011**, *47*, 6356.
(33) Kim, D. H.; Lee, D. Y.; Lee, H. S.; Lee, W. H.; Kim, Y. H.; Han, J. I.; Cho, K. *Adv. Mater.* **2007**, *19*, 678.
(34) Briseno, A. L.; Mannsfeld, S. C. B.; Ling, M. M.; Liu, S. H.; Tseng, R. J.; Reese, C.; Roberts, M. E.; Yang, Y.; Wudl, F.; Bao, Z. N. *Nature* **2006**, *444*, 913.
(35) Mannsfeld, S. C. B.; Sharei, A.; Liu, S. H.; Roberts, M. E.; McCulloch, I.; Heeney, M.; Bao, Z. A. *Adv. Mater.* **2008**, *20*, 4044.
(36) Liu, S. H.; Wang, W. C. M.; Briseno, A. L.; Mannsfeld, S. C. E.; Bao, Z. N. *Adv. Mater.* **2009**, *21*, 1217.
(37) Pisula, W.; Menon, A.; Stepputat, M.; Lieberwirth, I.; Kolb, U.; Tracz, A.; Sirringhaus, H.; Pakula, T.; Mullen, K. *Adv. Mater.* **2005**, *17*, 684.
(38) Li, L. Q.; Gao, P.; Schuermann, K. C.; Ostendorp, S.; Wang, W. C.; Du, C. A.; Lei, Y.; Fuchs, H.; De Cola, L.; Mullen, K.; Chi, L. F. *J. Am. Chem. Soc.* **2010**, *132*, 8807.
(39) Becerril, H. A.; Roberts, M. E.; Liu, Z. H.; Locklin, J.; Bao, Z. N. *Adv. Mater.* **2008**, *20*, 2588.
(40) Anthony, J. E.; Brooks, J. S.; Eaton, D. L.; Parkin, S. R. *J. Am. Chem. Soc.* **2001**, *123*, 9482.
(41) Uemura, T.; Hirose, Y.; Uno, M.; Takimiya, K.; Takeya, J. *Appl. Phys. Express* **2009**, *2*, 111501.
(42) Wang, L.; Liu, B. B.; Yu, S. D.; Yao, M. G.; Liu, D. D.; Hou, Y. Y.; Cui, T.; Zou, G. T.; Sundqvist, B.; You, H.; Zhang, D. K.; Ma, D. G. *Chem. Mater.* **2006**, *18*, 4190.
(43) Park, C.; Song, H. J.; Choi, H. C. *Chem. Commun.* **2009**, 4803.
(44) Chua, L. L.; Zaumseil, J.; Chang, J. F.; Ou, E. C. W.; Ho, P. K. H.; Sirringhaus, H.; Friend, R. H. *Nature* **2005**, *434*, 194.
(45) Wei, P.; Oh, J. H.; Dong, G. F.; Bao, Z. N. *J. Am. Chem. Soc.* **2010**, *132*, 8852.
(46) Kroto, H. W.; Heath, J. R.; Obrien, S. C.; Curl, R. F.; Smalley, R. E. *Nature* **1985**, *318*, 162.
(47) Chung, Y.; Verploegen, E.; Vailionis, A.; Sun, Y.; Nishi, Y.; Murmann, B.; Bao, Z. N. *Nano Lett.* **2011**, *11*, 1161.
(48) Najafov, H.; Lee, B.; Zhou, Q.; Feldman, L. C.; Podzorov, V. *Nat. Mater.* **2010**, *9*, 938.
(49) Zhang, Y. J.; Dong, H. L.; Tang, Q. X.; Ferdous, S.; Liu, F.; Mannsfeld, S. C. B.; Hu, W. P.; Briseno, A. L. *J. Am. Chem. Soc.* **2010**, *132*, 11580.